CARBON 76 (2014) 401–409

Available at www.sciencedirect.com

ScienceDirect

journal homepage: www.elsevier.com/locate/carbon

New developments in the growth of 4 Angstrom carbon nanotubes in linear channels of zeolite template

Qihong Chen [a], Zhe Wang [a], Yuan Zheng [a], Wu Shi [a], Dingdi Wang [a], Yi-Chia Luo [b], Bing Zhang [a], Jianming Lu [a], Haijing Zhang [a], Jie Pan [a], Chung-Yuan Mou [b], Zikang Tang [a], Ping Sheng [a,*]

[a] Department of Physics, Hong Kong University of Science and Technology, Clear Water Bay, Kowloon, Hong Kong
[b] Department of Chemistry, National Taiwan University, Taipei, Taiwan

ARTICLE INFO

Article history:
Received 5 February 2014
Accepted 30 April 2014
Available online 10 May 2014

ABSTRACT

We report new developments on the chemical vapor deposition growth of 0.4 nm single-walled carbon nanotubes (SWCNTs) inside the linear channels of the aluminophosphate zeolite, $AlPO_4$-5 (AFI), single crystals (0.4 nm-SWCNT@AFI). Ethylene (C_2H_4) and carbon monoxide (CO) were used as the feedstock. Polarized Raman spectroscopy was used to analyze the structure and quality of SWCNTs, both the radial breathing mode and G-band are much clearer and stronger than the samples grown by the old process which used template tripropylamine molecules for growing SWCNT@AFI. From the Raman spectra, it is clearly seen that the RBM is composed of two peaks at 535 and 551 cm^{-1}. By using the pseudopotential module in Material Studio to calculate the Raman lines, the 535 cm^{-1} peak is attributed to the (5,0) SWCNTs and the 551 cm^{-1} peak to the (3,3) SWCNTs. The abundance of (4,2) is relatively small. Thermal gravity analysis showed that while the samples grown by CO display less than 1 wt% of carbon, for the samples heated in C_2H_4 atmosphere the weight percentage of SWCNTs is around 10%, which implies ~30% of the AFI channels are occupied with SWCNTs, a significant increase compared with the previous samples.

1. Introduction

Carbon nanotubes (CNTs) have been intensively studied since their discovery [1,2]. Owing to their unique physical properties and the one-dimensional character, they are regarded as one of the basic materials of the nanotechnology industry [3–6]. Much effort has been devoted to the synthesis of desirable chirality (n,m) single-walled carbon nanotubes (SWCNTs) at a given location, with well-controlled direction and length [7–11]. Compared with large-sized SWCNTs, ultra-small SWCNTs have aroused special interests because of the strong curvature effect that can lead to a significant hybridization between the sigma (σ^*) and pi (π^*) orbitals [12]. The curvature effect enriches the electronic properties by redistributing the energy in the electronic states, and opens new channels for electron–phonon coupling which can lead to special transport characteristics. However, SWCNTs with very small diameter can become unstable, as the system energy increases

* *Corresponding author:* Fax: +852 2358 1652.
E-mail address: sheng@ust.hk (P. Sheng).
http://dx.doi.org/10.1016/j.carbon.2014.04.094
0008-6223/

rapidly with decreasing diameter [13]. Theoretical calculations predicted the existence of SWCNTs with diameter as small as 0.4 nm [14]. Later it was reported that the ultra-small SWCNTs can be produced inside the channels of aluminophosphate, $AlPO_4$-5 (AFI), zeolite single crystals [15], and the diameter was determined to be 0.4 nm by high resolution transmission electron microscopy [16]. With such a small diameter and extreme curvature, these well-aligned and mono-sized SWCNT arrays showed interesting physical properties, e.g. superconductivity has been observed in this system [17–21].

The host AFI zeolite crystal is a type of microporous aluminophosphate zeolites. It is widely used in the host–guest chemistry because of its thermal stability up to 1200 °C, optical transparency over the broad range ultraviolet to near infrared, and electrically insulating characteristic [22–26]. Fig. 1 shows the structure of the AFI crystal viewed along the [001] (c-axis) direction. The framework is composed of alternating tetrahedral $(AlO_4)^-$ and $(PO_4)^+$ units, forming parallel open channels that are arranged in a triangular lattice structure [27]. The inner diameter of the channel is 0.734 nm and the center-to-center distance between two neighboring channels is 1.374 nm. The tripopylamine $[(CH_3CH_2CH_2)_3N$ (TPA)] molecules are aligned head-to-tail along the c-axis, serving as the precursor template while synthesizing the AFI crystals. In the old method of producing the 0.4 nm CNTs, the SWCNTs were obtained by pyrolyzing the TPA molecules [15]. The AFI crystals were heated to 580 °C in vacuum for several hours, leading to the decomposition of the TPA molecules that are encapsulated inside the AFI channels, with a small fraction forming the SWCNTs. There are limitations for this process: In Raman spectroscopy the intensity of the radial breathing mode (RBM) is weak and the peaks are broad; the thermal gravity analysis (TGA) data showed the weight percentage of carbon over the total mass of SWCNT@AFI crystal to be ~1.5 wt%, translating into a filling factor of SWCNTs inside the AFI channels of ~4.5%. This is a relatively small number, indicating that the samples are not uniform and only a small fraction of AFI channels are occupied with SWCNTs. In this approach, the carbon atoms that formed the SWCNTs came from the pyrolysis of the TPA molecules inside the AFI channels. Since the total amount of TPA molecules are limited in quantity and some of them may escape during the heating process (the AFI crystals were heated in vacuum), the low filling factor is understandable.

To improve this situation, we have developed a new chemical vapor deposition (CVD) process by first burning off the TPA molecules in oxygen atmosphere, and then introducing carbon-containing gas as the feedstock. Two gases were tested: C_2H_4 and CO. In this approach, continuous carbon source can enter the empty channels of the AFI crystals. Compared with the traditional CVD method for growing CNTs, no catalyst is used in the present process. The fact that CNTs can still be formed suggests that the framework of AFI crystal must play a weak catalytic role in the pyrolysis and conversion of ethylene, or CO, to SWCNTs.

2. Experimental

The AFI zeolite crystals are synthesized by the conventional hydrothermal method. In the synthesis procedure, aluminum tri-isopropoxide $[(iPrO)_3Al$ 99 wt%] and phosphoric acid (H_3PO_4 85 wt%) were used as aluminum and phosphorus sources, respectively. The TPA molecules served as the template during the synthesis process. The details are described in reference [28]. The as-grown AFI crystals, with TPA molecules capsulated in the channels, are optically transparent with a typical dimension of 300 μm in length and 100 μm in diameter.

The as-made AFI crystals are first heated in a flowing oxygen atmosphere at 900 °C, to remove the organic template TPA molecules through oxidization. Raman spectroscopy of the AFI crystals after this step showed no RBM or G band, which means that the channels of the AFI crystals are mostly empty and ready for the growth of SWCNT. Subsequently, a

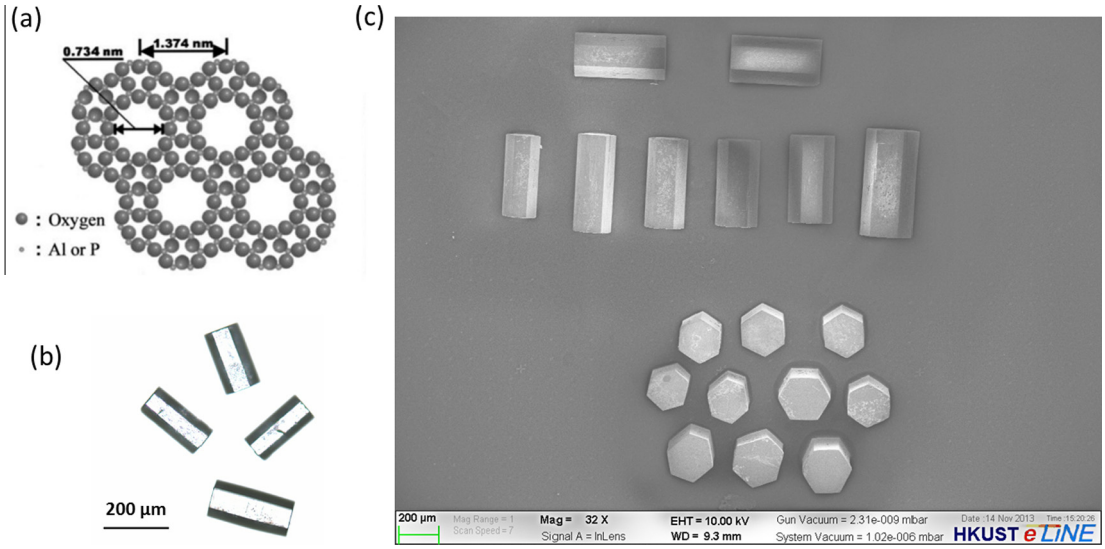

Fig. 1 – The (a) framework, (b) optical and (c) SEM images of AFI zeolite crystals. (A color version of this figure can be viewed online.)

flowing gas mixture of C_2H_4 (or CO) and nitrogen was introduced for growing the SWCNT, while the heating temperature was controlled within the range of 600–950 °C. In theory, perfect AFI crystal is stable up to 1200 °C, so we have tried heating temperatures higher than 950 °C with CO. The resulting quality of the sample was poor, however, because in reality the AFI crystals have defects, which tend to degrade the crystals before the stability temperature is reached. Hence the heating temperature was controlled to be below 950 °C. After the heating treatment, the AFI crystals appear dark brown in color and exhibit strong optical anisotropy; i.e., almost transparent (black) when the electric field is perpendicular (parallel) to the *c*-axis.

The SWCNT@AFI were characterized by polarized Raman spectroscopy using a Jobin Yvon T6400 3000 micro-Raman system and 514.5 nm Ar laser excitation at room temperature. Thermo-gravimetry analyses were carried out by a thermal analysis apparatus (STA 449C Jupiter) to characterize the carbon content inside the AFI channels.

3. Results and discussion

Several hundreds of heating processes were carried out by varying the heating temperature, gas pressure, gas flow rate, and carbon source. Overall, they can be categorized into three groups: (I) the old process which used TPA molecules as the carbon source for growing SWCNTs; (II) new CVD process with CO being the carbon source for SWCNTs; and (III) new CVD process with C_2H_4 being the carbon source. The results can vary significantly. In Fig. 2, we choose one representative sample in each group to display their Raman spectra. The associated heating processes of the three batches of SWCNT@AFI are shown in Fig. 3.

The P–O and P–O–Al vibrations of the AFI framework give rise to signals at 450 and 1100 cm^{-1} in the Raman spectra,

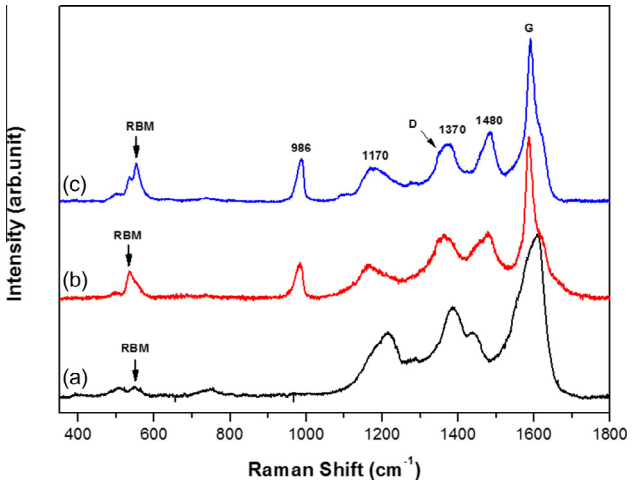

Fig. 2 – The Raman spectra of 0.4 nm-SWCNT@AFI samples fabricated by the old process (I), shown as the black curve (a); new CVD process with CO (II), shown as the red curve (b); and new CVD process with C_2H_4 (III), shown as the blue curve (c). (A color version of this figure can be viewed online.)

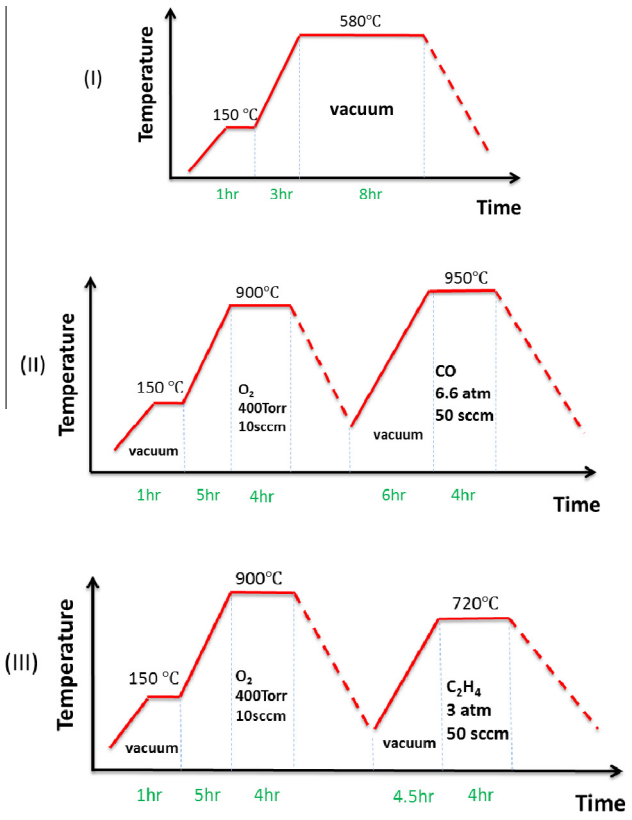

Fig. 3 – Detailed heating processes of the three batches of samples whose Raman spectra are shown in Fig. 2. (A color version of this figure can be viewed online.)

but they are normally very weak compared with the signals from the SWCNTs [30]. Hence the effect of the AFI framework can be neglected in the Raman spectra. It can be seen that although the SWCNTs were grown from different sources, their Raman spectra have very similar features. Especially for the samples grown by the new CVD process with ethylene or CO source, their spectra coincide quite well with each other. They differ only in some small but notable features. Below we comment on the various features of the Raman spectra.

(1) The radial breathing mode is in the low frequency region of 500–600 cm^{-1}. The RBM serves as an unique signature of CNTs because it corresponds to the coherent vibration of the carbon atoms along the radial direction. Planar structures such as graphene or graphite do not have such Raman-active modes. The RBM of SWCNTs fabricated by the new CVD process (II) or (III) is much more evident than that of (I), thereby they provide us more information about the structure of the SWCNTs. According to the high resolution TEM characterization [16], the diameter of the SWCNT@AFI was determined to be 0.4 nm. There are only three possible SWCNTs with such a small diameter: the zigzag (5,0), the armchair (3,3) and the chiral (4,2)

Since not all the carbon atoms in the AFI channels must be in the nanotube form, some of them can be in the form of

amorphous carbon which will give rise to G-band signal but no RBM signal. So the RBM/G ratio can serve as a simple yet intuitive indication of the amount of carbon atoms that is in the nanotube form. However, it should be noted that the RBM/G ratio is not necessarily related to the TGA result, since the latter indicates the total amount of carbon, rather than its distribution among the amorphous form or the nanotube form. Fig. 4 shows the results of a statistical study on the RBM/G band ratio, for the three batches of samples shown in Fig. 2. We can see that the RBM/G ratio increased greatly from ~5% (sample I) to almost ~20% (sample III). This clearly suggests that for the new fabrication process, there is less amorphous carbon in the AFI channels.

(2) G band is an important feature of CNTs. For SWCNTs, the G band consists of two main components as shown in Fig. 5(a): G^+ and G^-, corresponding to the movement of carbon atoms along the tube axis and the circumferential direction, respectively. From Fig. 5(b), we can see that the G^+ band of the 0.4 nm-SWCNT@AFI is exactly at 1590 cm^{-1} and can be fitted with the Lorentzian line shape very well, in good agreement with the larger diameter SWCNTs reported elsewhere [31,32]. There is a small peak around 1614 cm^{-1}. This may be due to the tangential mode of semiconducting nanotubes composed of a few Lorentzians [31]. This also shows that the G^+ peak is independent of the tube diameter, even down to 0.4 nm. Besides, the G^+ band is very sharp compared with that from samples fabricated by process (I)

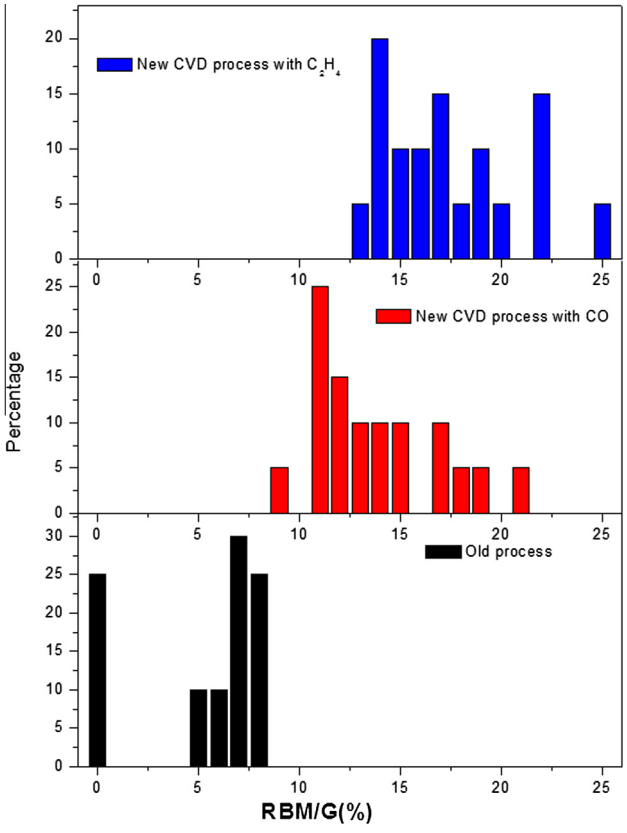

Fig. 4 – Statistics of RBM/G ratio for samples fabricated by the three different processes. (A color version of this figure can be viewed online.)

In contrast to the G^+ peak, the frequency and line shape of the lower frequency G^- peak are strongly related to the chirality and diameter of the nanotubes. The G^- band of armchair carbon nanotube have a Breit–Wigner–Fano (BWF) line shape (a broad and asymmetric peak), while the G^- band of the semiconducting carbon nanotubes remains Lorentzian [33,34]. In accordance with the density functional theory (DFT) calculation of the electronic band structure, the (5,0) SWCNTs are metallic because of its small radius [35]. However, from the zone folding approach [36] or the tight binding calculations [37], the zigzag (5,0) nanotubes are semiconducting in character. For the Raman characteristics, we should therefore examine both the metallic and semiconducting characteristics of the G^- band.

For armchair SWCNTs, the frequency of G^- band is related to its diameter by the relation [31]:

$$\omega_G^- = \omega_G^+ - \frac{C}{d_t^2}, \tag{1}$$

with $C = C_M = 79.5\ cm^{-1}\ nm^2$. According to Eq. (1), the frequency of the G^- band should be around 1100 cm^{-1} for the metallic armchair 0.4 nm-SWCNT@AFI. In the Raman spectra of SWCNT@AFI there is a broad peak around 1170 cm^{-1}, and in Fig. 5(c) we see that it fits well with the BWF line shape. So this peak can very well be the G^- band of armchair 0.4 nm-SWCNT@AFI. The deviation from what is predicted by Eq. (1) can be due to the strong curvature effect of the 0.4 nm tube structure.

For the non-armchair SWCNTs, six Raman-active modes of $A + E_1 + E_2$ symmetry, along each of the two orthogonal (the axial and circumferential) directions, can be present in the G band [38]. The frequency of the G^- band for the semiconducting SWCNTs can be well fitted by the relation:

$$\omega_G^- = 1592 - \frac{C}{d_t^\beta}, \tag{2}$$

With $\beta = 1.4$, $C_{E_2} = 64.6\ cm^{-1}\ nm^{1.4}$, $C_A = 41.4\ cm^{-1}\ nm^{1.4}$, and $C_{E_1} = 32.6\ cm^{-1}\ nm^{1.4}$ [39]. According to Eq. (2), the G^- peaks should be at 1359 (E_2), 1443 (A), and 1474 cm^{-1} (E_1) for the non-armchair 0.4 nm-SWCNT@AFI. From the Raman spectra fitting of sample (III) in Fig. 5(d), four peaks centered at 1352, 1377, 1460, 1483 cm^{-1} are identified. The 1352 cm^{-1} should be associated with the disorder induced D band which will be discussed in the next section. It is tempting to attribute the remaining three peaks to the G^- band of semiconducting 0.4 nm-SWCNT@AFI. However, from the polarized Raman spectra shown in Fig. 6, The 1377 cm^{-1} mode not only exhibit strong intensity at (ZZ) and (XX) polarized spectra associated with the $A_1(A_{1g})$ symmetry, but also has intensities in cross-polarized (ZX) and (XZ) spectra indicating that it should be assigned the $E_1(E_{1g})$ symmetry, but the frequency is too far from the predicted E_1 mode at 1474 cm^{-1}. The 1460 and 1483 cm^{-1} peaks are observed in the (ZZ) and (XX) parallel polarized spectra, hence they should be assigned $A_1(A_{1g})$ symmetry. Whereas 1460 cm^{-1} is close to the 1443 cm^{-1} G^- mode with the correct symmetry, the other

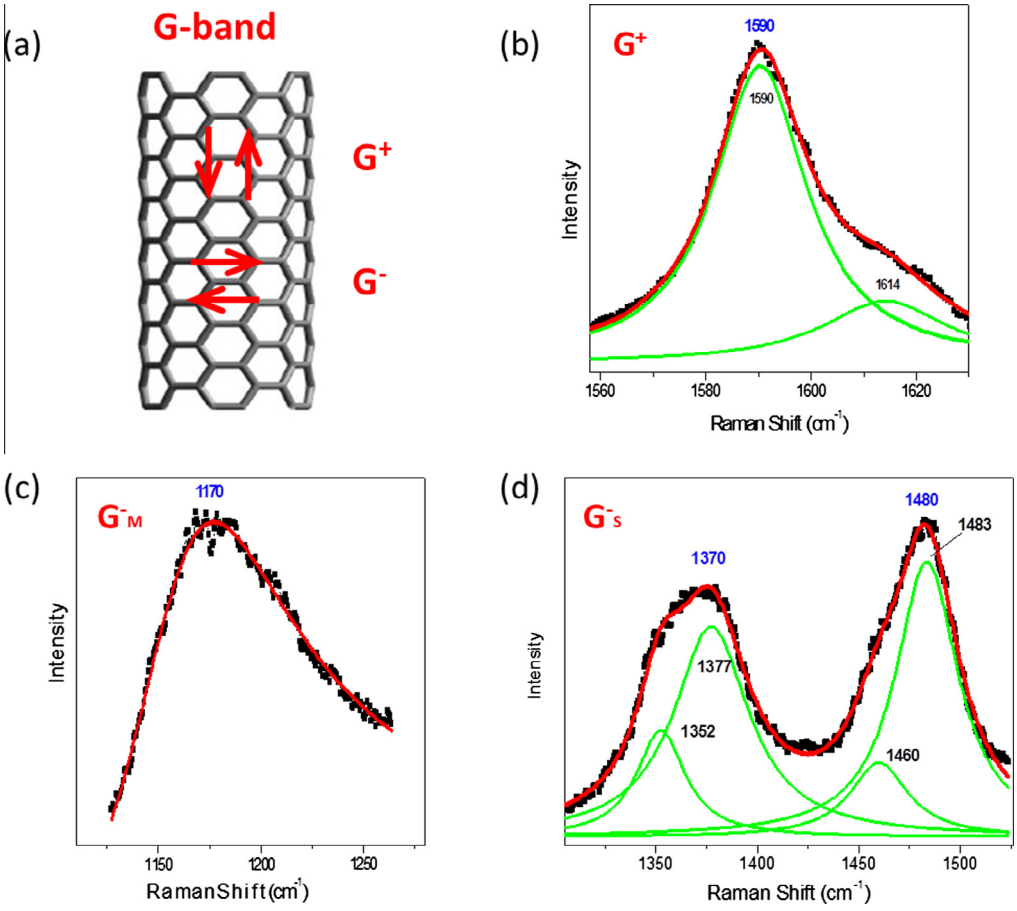

Fig. 5 – (a) Two types of vibrations for the G band. (b) Fitting of the G band of sample III at 1590 cm^{-1} by the Lorentzian line shape. (c) Fitting of the G^-_M band at 1170 cm^{-1} by the BWF line shape. (d) Fitting of the G^-_S band at 1370 and 1480 cm^{-1} by the Lorentzian line shape. (A color version of this figure can be viewed online.)

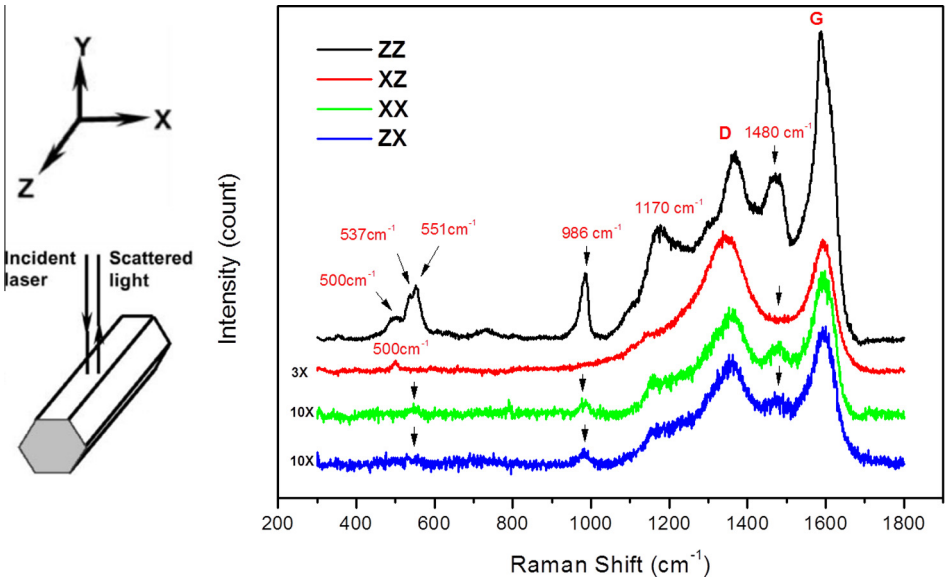

Fig. 6 – Polarized Raman spectra of the SWCNT@AFI. Y direction denotes the incident light direction and the Z direction denotes the c-axis direction of SWCNT. The XZ, XX and ZX configurations are enlarged, and vertically shifted, for comparison. This batch of sample was heated with the C_2H_4 under the condition of pressure = 400 Torr and temperature = 700 °C for 4 h, but it showed similar Raman behavior with sample (III) fabricated under higher temperature and pressure, even though the carbon content is much lower as evidenced by the TGA. (A color version of this figure can be viewed online.)

one, at 1483 cm^{-1}, cannot be easily identified so far. It should be noted that Eq. (2) is obtained by measuring the Raman spectra of isolated SWCNTs [39], but the Raman spectra of 0.4 nm-SWCNT@AFI are measured within the framework of the AFI crystals. Thus some frequency difference may be attributed to the interactions between the nanotube and the AFI framework.

(3) As mentioned above, there is a D band around 1352 cm^{-1}, which might be due to defects in the tube structure. It should be noted that the Raman spectra was measured with half of the crystal milled away by mechanical polishing, which means the surface amorphous carbon was removed. A higher D band peak would correspond to a higher concentration of defects in the sample. Different fabrication conditions have been tested to minimize the D band, but the intensity is still relatively large. It is speculated that the D band might also arise from the curvature effect, owing to the small radius.

(4) There is a sharp, asymmetric peak at 986 cm^{-1}. From Fig. 6 we can see that the 986 cm^{-1} peak always accompanies the RBM: It is weak when the RBM is weak (both the XX and ZX configurations); and it disappears when the RBM is absent (XZ configuration). Previous study on the intermediate frequency region modes (between 600 and 1100 cm^{-1}) of larger diameter SWCNTs (d_t = 1.5 ± 0.3 nm) has revealed that this peak can be related to the combination of one optical and one acoustic phonon that originate from a zone folding procedure of two 2D phonon braches, associated with *the out-of-plain vibrations* of carbon atoms [40]. Such mode is Raman-inactive for large carbon nanotubes, but can be active for small diameter carbon nanotubes. However, the intensity of this mode for the 4-Angstrom carbon nanotubes is still to be pursued.

We note that another feature in Fig. 6 is the peak at 500 cm^{-1}. It is independent of the RBM and is clear and sharp for the XZ configuration. It also appears in the Raman spectra of the empty AFI crystals after the TPA molecules were removed by heating in oxygen atmosphere. So the peak at 500 cm^{-1} should be associated with the AFI framework, not related to the SWCNTs.

Fig. 7 shows the RBM of the samples from three different processes. From (II) and (III) it is seen that the RBM is composed of two peaks at 535 and 551 cm^{-1}. The broad peak around 500 cm^{-1}, which is very weak compared with other peaks, is attributed to the framework of AFI crystal as discussed above. For our template-grown carbon nanotubes, there are only three candidates with suitable diameters: (5,0), (3,3) and (4,2), with the respective diameters of 0.393, 0.407 and 0.414 nm. Since the diameter of the AFI channels is 0.73 ± 0.01 nm and the distance between the wall of SWCNTs and the AFI channels should be close to the separation between graphite sheet (0.34 nm), the allowed diameter is 0.39 ± 0.01 nm. So the diameters of the (5,0) and (3,3) are more favorable than (4,2). In addition, it is reported that by using CO, the growth of the (10,0) zigzag tubes is more favorable than the (5,5) armchair tubes [41]. This may suggest that zigzag tubes can be preferred in the growth using CO gas. In Fig. 7 we can see that for the 0.4 nm-SWCNT@AFI fabricated by CO gas, the peak at 535 cm^{-1} is stronger than that at 551 cm^{-1}. So the peak at 535 cm^{-1} is attributed to (5,0), and the peak at 551 cm^{-1} is attributed to the (3,3) carbon nanotubes. This assignment is further supported by theory calculations, shown below. The signal from (4,2), if it exists, must be very weak.

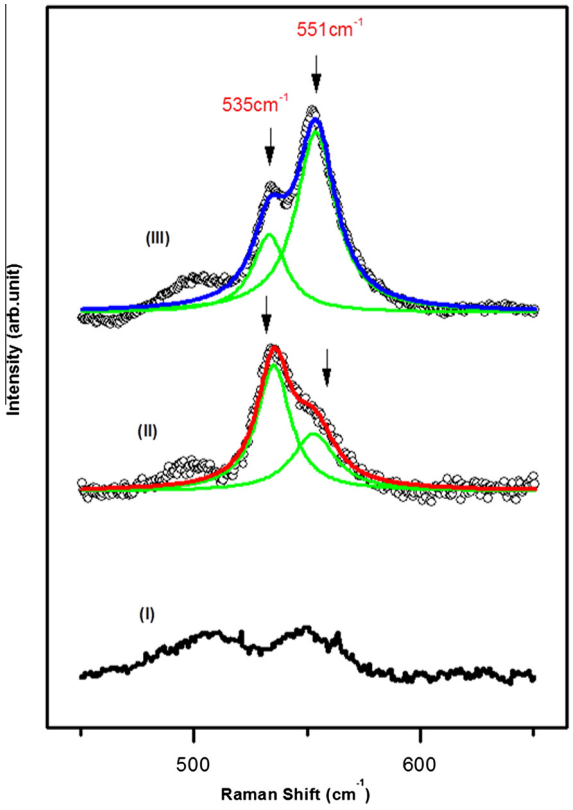

Fig. 7 – RBM of the three processes from Fig. 2: (I) old process; (II) CVD process with CO; (III) CVD process with C_2H_4. (A color version of this figure can be viewed online.)

We have carried out the calculation of RBM for the (5,0), (3,3) and (4,2) nanotubes by using the CASTEP pseudopotential module in Material Studio. The results are listed in Table 1.

From Table 1, the RBMs of (3,3), (5,0), (4,2) are at 556.7, 534.9, and 526 cm^{-1}, respectively. Although the frequency of RBM may change a few wave numbers when different pseudopotential is used, their differences are fixed relative to each other. The calculated results therefore agree well with our previous assignment that the peaks at 551 and 535 cm^{-1} belong to (3,3), (5,0), respectively, and that (4,2) is hardly seen in the 0.4-nm SWCNT@AFI system. Hence it may be possible to develop a chirality-selective process of growing SWCNTs using CO.

Thermal-gravimetric analysis was carried out to characterize the quantity of SWCNTs inside the channels of AFI crystals. The TGA result of sample (III) is shown in Fig. 8. The weight loss, starting at around 570 °C, is attributed to the

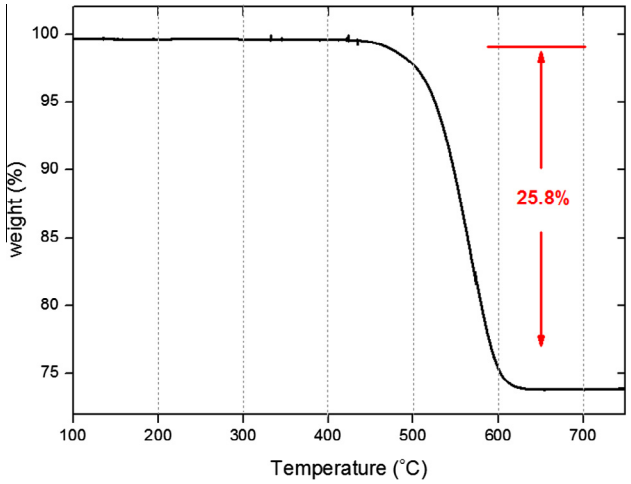

Fig. 8 – Thermogravimetric data from 18 mg of 0.4 nm-SWCNT@AFI obtained from process (III) in flowing oxygen, with a ramp rate of 5 °C/min. (A color version of this figure can be viewed online.)

oxidation of carbon. We see that by using ethylene as the carbon feedstock and heating under high pressure condition the total weight percentage of carbon can reach 25.8 wt%. However, the weight percentage of SWCNTs should be smaller than the total weight loss because there is amorphous carbon on the surface of the AFI crystals. Normally the oxidization temperature of amorphous carbon should be lower than that of SWCNTs, but for our case they are very close. We have measured the TGA of amorphous carbon, collected from the quartz tube after growing the 0.4 nm-SWCNT@AFI. The results are shown in Supplementary Materials [29]. They confirm that in our case, the oxidization temperature of amorphous carbon is higher than what might be usually expected, most probably owing to the relatively high heating pressure and temperature under which the amorphous carbon was formed, leading to a more tightly-packed, highly linked structure that is more robust against oxidation. The thickness of the amorphous carbon layer was measured to be ~2.5 μm. By taking into account the density of amorphous carbon – 2.0 g/cm^3, density of AFI crystals – 2.6 g/cm^3, and the average size of the crystals – 300 μm in length and 100 μm in diameter; the weight percentage of amorphous carbon is estimated to be 15%. That means the contribution from SWCNTs is approximately 10%, which is much higher than the value obtained the old process (I).

Table 2 – Carbon content and pore filling factor of samples from the three processes.

Pressure	Carbon content (%)	Pore filling factor (%)
Process (I)	1.5	4.5
Process (II)	0.7	2.1
Process (III)	10.0	30.0

Although the carbon content is greatly increased, by calculation it is inferred that not every channel is filled with CNTs. We define the filling factor as the percentage of the channel space occupied by SWCNTs over the total amount of channel space. The carbon content and filling factor are listed in Table 2. From the table we can see that when we use ethylene as carbon source and heat under high pressure (III), the carbon content can be increased from 1.47% to 10% as compared to the old process (I), with the filling factor increasing from 4.5% to 30%.

We note that the carbon content of SWCNT@AFI heated by process (II), using CO, is about 0.7%, much lower than both process (III) and (I). This may be due to the fact that CO is more stable than either ethylene or TPA, and no catalyst was used in the heating process. Without a catalyst, it may be difficult for CO to decompose and form SWCNTs in the AFI channels. By using CO as the carbon source and heating under high pressure, there are some good SWCNTs in local areas of AFI crystals, but the overall amount of SWCNTs is still small.

We show in Fig. 9 a two dimensional summary of results, with ethylene gas as the feedstock. Here pressure is the vertical axis and heating temperature serves as the horizontal axis. The old process is noted to yield samples with only very weak RBMs and small amount of nanotubes in the channels.

Table 1 – The RBM of (3,3), (5,0), (4,2) as calculated by the CASTEP pseudopotential module in Material Studio. The green arrows indicate the directions of motion.

Radial Breathing Eigenmode	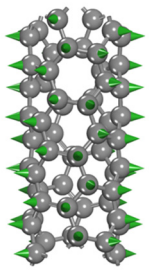	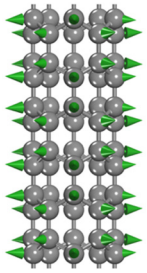	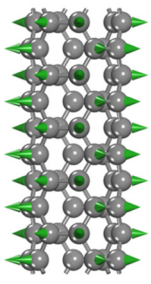
chirality	(4,2)	(5,0)	(3,3)
Raman Shift (cm^{-1})	526	534.9	556.7

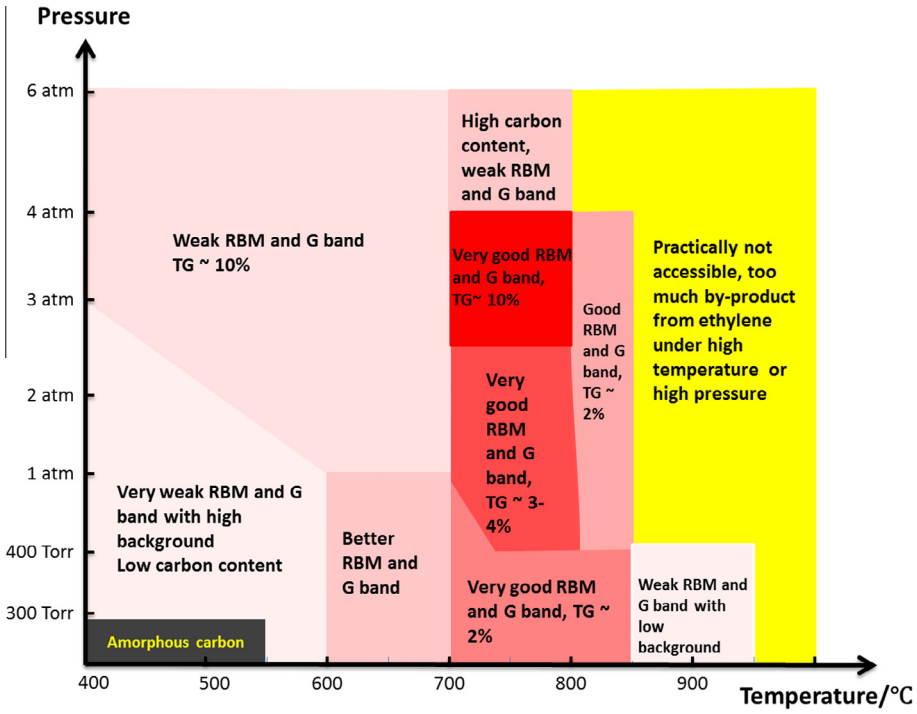

Fig. 9 – Overall result of different heating conditions for process (III), using ethylene as the feedstock. (A color version of this figure can be viewed online.)

The use of CO without catalyst, on the other hand, leads to good RBM signals but very small pore filling. Thus the optimal approach is to use ethylene as the carbon source, with the conditions delineated by the dark red area in Fig. 9. The difficulty of using ethylene as the source, however, is that at temperatures higher than 800 °C the polymerizing tendency of the ethylene molecules can lead to the proliferation of by-products in both liquid and solid form. When that happens, the AFI crystals can be difficult to extract from the resulting (fused) mixture.

4. Conclusion

By taking advantage of the small channels of AFI crystals, we have developed an efficient CVD process of growing uniform 0.4 nm-SWCNTs using ethylene and CO. This new process is better than the old process as evidenced by the Raman spectra showing that both the RBM and G band to be clearer and stronger than the old process. The two clear RBM peaks at 535 and 551 cm^{-1} indicate that the 0.4 nm-SWCNT@AFI are mainly composed of (5,0) and (3,3) nanotubes. This conclusion is supported by theoretical calculations. Our results also suggest the possibility of developing a chirality-selective growing process of 0.4 nm-SWCNT@AFI using CO. By using ethylene as the feedstock and heating under high pressure with a temperature of 700 °C, both the quantity and quality of 0.4 nm-SWCNTs in the AFI channels are significantly improved.

Acknowledgments

This work has been supported by the Research Grants Council of Hong Kong, Grants HKUST9/CRF/08 and CA04/04.SC02. C.Y.M. and Y.J.L. wish to thank the support by the Research Grants of Taiwan, Grants NSC 100-2120-M-002-011 and NTU-CESRP-102R7621.

Appendix A. Supplementary data

Supplementary data associated with this article can be found, in the online version, at http://dx.doi.org/10.1016/j.carbon.2014.04.094.

REFERENCES

[1] Oberlin A, Endo M, Koyama T. Filamentous growth of carbon through benzene decomposition. J Cryst Growth 1976;32(3):335–49.
[2] Iijima S. Helical microtubules of graphitic carbon. Nature 1991;354(6348):56–8.
[3] Saito R. Physical properties of carbon nanotubes (paperback). 1998.
[4] Charlier J-C, Blase X, Roche S. Electronic and transport properties of nanotubes. Rev Mod Phys 2007;79(2):677.
[5] Dresselhaus MS, Dresselhaus G, Eklund P, Rao A. Carbon Nanotubes. Springer; 2000.
[6] Baughman RH, Zakhidov AA, de Heer WA. Carbon nanotubes – the route toward applications. Science 2002;297(5582):787–92.
[7] Dai H. Carbon nanotubes: synthesis, integration, and properties. Acc Chem Res 2002;35(12):1035–44.
[8] Hanus MJ, Harris AT. Synthesis, characterisation and applications of coiled carbon nanotubes. J Nanosci Nanotechnol 2010;10(4):2261–83.
[9] Awasthi K, Srivastava A, Srivastava O. Synthesis of carbon nanotubes. J Nanosci Nanotechnol 2005;5(10):1616–36.

[10] Tan L-L, Ong W-J, Chai S-P, Mohamed AR. Growth of carbon nanotubes over non-metallic based catalysts: a review on the recent developments. Catal Today 2013;217:1–12.
[11] Azam MA, Manaf NSA, Talib E, Bistamam MSA. Aligned carbon nanotube from catalytic chemical vapor deposition technique for energy storage device: a review. Ionics 2013;19(11):1455–76.
[12] Blase X, Benedict LX, Shirley EL, Louie SG. Hybridization effects and metallicity in small radius carbon nanotubes. Phys Rev Lett 1994;72(12):1878.
[13] Robertson D, Brenner D, Mintmire J. Energetics of nanoscale graphitic tubules. Phys Rev B 1992;45(21):12592.
[14] Sawada S, Hamada N. Energetics of carbon nanotubes. Solid State Commun 1992;83(11):917–9.
[15] Tang ZK, Sun HD, Wang J, Chen J, Li G. Mono-sized single-wall carbon nanotubes formed in channels of AlPO4-5 single crystal. Appl Phys Lett 1998;73(16):2287–9.
[16] Wang N, Tang Z-K, Li G-D, Chen J. Materials science: single-walled 4 Å carbon nanotube arrays. Nature 2000;408:50–1.
[17] Wang Z, Shi W, Xie H, Zhang T, Wang N, Tang Z, et al. Superconducting resistive transition in coupled arrays of 4 Å carbon nanotubes. Phys Rev B 2010;81(17):174530.
[18] Lortz R, Zhang Q, Shi W, Ye JT, Qiu C, Wang Z, et al. Superconducting characteristics of 4-Å carbon nanotube–zeolite composite. Proc Natl Acad Sci 2009;106(18):7299–303.
[19] Zhang T, Sun MY, Wang Z, Shi W, Sheng P. Crossover from Peierls distortion to one-dimensional superconductivity in arrays of (5,0) carbon nanotubes. Phys Rev B 2011;84(24):245449.
[20] Wang Z, Shi W, Lortz R, Sheng P. Superconductivity in 4-Angstrom carbon nanotubes – a short review. Nanoscale 2012;4(1):21–41.
[21] Sun M, Hou Z, Zhang T, Wang Z, Shi W, Lortz R, et al. Dimensional crossover transition in a system of weakly coupled superconducting nanowires. New J Phys 2012;14(10):103018.
[22] Terasaki O, Yamazaki K, Thomas J, Ohsuna T, Watanabe D, Sanders J, et al. Isolating individual chains of selenium by incorporation into the channels of a zeolite. Nature 1987;330(6143):58–60.
[23] Cox S, Gier T, Stucky G. Second harmonic generation by the self-aggregation of organic guests in molecular sieve hosts. Chem Mater 1990;2(5):609–19.
[24] Wu C-G, Bein T. Conducting polyaniline filaments in a mesoporous channel host. Science 1994;264:1757–9.
[25] Li IL, Tang Z. Structure study of Se species in channels of $AlPO_4$-5 crystals. Appl Phys Lett 2002;80(25):4822–4.
[26] Marlow F, Hoffmann K, Caro J. Photoinduced switching in nanocomposites of azobenzene and molecular sieves. Adv Mater 1997;9(7):567–70.
[27] Wilson ST, Lok BM, Messina CA, Cannan TR, Flanigen EM. Aluminophosphate molecular sieves: a new class of microporous crystalline inorganic solids. J Am Chem Soc 1982;104(4):1146–7.
[28] Zhai J, Li Z, Liu H, Li I, Sheng P, Hu X, et al. Catalytic effect of metal cations on the formation of carbon nanotubes inside the channels of $AlPO_4$-5 crystal. Carbon 2006;44(7):1151–7.
[29] See Supplementary Material for Characterization of the by-product amorphous carbon.
[30] Tang Z-K, Wang N, Zhang X, Wang J, Chan C-T, Sheng P. Novel properties of 0.4 nm single-walled carbon nanotubes templated in the channels of AlPO4-5 single crystals. New J Phys 2003;5(1):146.
[31] Jorio A, Souza Filho A, Dresselhaus G, Dresselhaus M, Swan A, Ünlü M, et al. G-band resonant Raman study of 62 isolated single-wall carbon nanotubes. Phys Rev B 2002;65(15):155412.
[32] Dresselhaus M, Eklund P. Phonons in carbon nanotubes. Adv Phys 2000;49(6):705–814.
[33] Dresselhaus MS, Dresselhaus G, Saito R, Jorio A. Raman spectroscopy of carbon nanotubes. Phys Rep 2005;409(2):47–99.
[34] Barnett R, Demler E, Kaxiras E. Electron–phonon interaction in ultrasmall-radius carbon nanotubes. Phys Rev B 2005;71(3):035429.
[35] Liu H, Chan C. Properties of 4 Å carbon nanotubes from first-principles calculations. Phys Rev B 2002;66(11):115416.
[36] Dresselhaus M, Dresselhaus G, Jorio A, Souza Filho A, Saito R. Raman spectroscopy on isolated single wall carbon nanotubes. Carbon 2002;40(12):2043–61.
[37] Saito R, Dresselhaus G, Dresselhaus M. Trigonal warping effect of carbon nanotubes. Phys Rev B 2000;61(4):2981.
[38] Jorio A, Dresselhaus G, Dresselhaus M, Souza M, Dantas M, Pimenta M, et al. Polarized Raman study of single-wall semiconducting carbon nanotubes. Phys Rev Lett 2000;85(12):2617.
[39] Jorio A, Pimenta M, Souza Filho A, Samsonidze GG, Swan A, Ünlü M, et al. Resonance Raman spectra of carbon nanotubes by cross-polarized light. Phys Rev Lett 2003;90(10):107403.
[40] Fantini C, Jorio A, Souza M, Ladeira L, Souza Filho A, Saito R, et al. One-dimensional character of combination modes in the resonance Raman scattering of carbon nanotubes. Phys Rev Lett 2004;93(8):087401.
[41] Seo K, Kim C, Kim B, Lee YH, Song K. Growth energetics of single-wall carbon nanotubes with carbon monoxide. J Phys Chem B 2004;108(14):4308–13.